Bone Reports 14 (2021) 101066

Contents lists available at ScienceDirect

Bone Reports

journal homepage: www.elsevier.com/locate/bonr

The normal stiffness of the edentulous alveolar process

S. Chen [a,*], D. Rittel [a], K. Shemtov Yona [a,b]

[a] Mechanical Engineering Faculty, Technion, Israel Institute of Technology, Haifa, Israel
[b] The Maurice and Gabriela Goldschleger School of Dental Medicine, Department of Oral Biology, Tel Aviv University, Tel Aviv, Israel

ARTICLE INFO

Keywords:
Jawbone stiffness
Bone classification
Trabecular-cortical interface
Structural synergy

ABSTRACT

The normal stiffness of the jawbone is seldom considered, as opposed to the mechanical properties of its individual cortical and trabecular components. Our standpoint is essentially structural, rather than purely material-oriented, as the jawbone is considered as a natural load-bearing structure. Throughout the work, 3 representative sections in the mandible and the maxilla are modelled and compared. Specifically, we evaluate the sections' elastic structural stiffness numerically, according to the recent geometrical classification proposed by Shemtov Yona (2021). Each case is modelled using two extreme configurations for the cortical-trabecular interaction, namely bonded and unbonded. Those two configurations reflect extreme interfacial conditions, though the bonded one is more physical. For the unbonded cases, the structural stiffness is the sum of the individual stiffnesses of the components. By sharp contrast, the bonded case results in a much larger stiffness than that obtained by the simple sum of the individual stiffnesses, indicating a strong synergistic stiffening effect between the components through their interface. We also investigate the role of the elastic moduli, whose reported values vary widely in the literature, emphasizing the role of the trabecular Poisson's coefficient, whose stiffening effect is evidenced when it exceeds about 0.3. The bone's structural stiffness shown here complements the geometrical classification of the jawbone types with a fundamental mechanical/structural property delineating the coupling between the mechanical properties and the geometry. The adopted approach is not limited to the jawbone and applies in principle to other bone types. From a clinical standpoint, the results presented here complement not only the basic mechanical aspects of the geometrical characterization, but also provide a starting point for future studies on dental implant placement and stability, the latter being directly related to the structural stiffness.

1. Introduction

Two major skeletal components make up the masticatory system, namely the maxilla (upper ridge) and the mandible (lower ridge). The alveolar processes, which harbor the teeth, are an integral part of these bones. Developmentally, the alveolar process in the maxilla and mandible extends from the basal bone during eruption of the teeth (Stanley and Major, 2010). While the maxilla ridge can be considered as part of the skull, the mobile mandible ridge is more complex, as it extends from the joint-connection to the skull through the condyle process, the coronoid and the ramus (Stanley and Major, 2010).

The alveolar process shape and architecture are biomechanically dictated by the shape of the teeth and the forces exerted on them. The alveolar ridges, in cross sections, form a non uniform U-shape housing the teeth. In the dentate jaw, the bony components include a thin cortical bone that envelops a trabecular bone. These two bone types, although similar in composition, differ by architecture and density and therefore in their mechanical properties (Natali, 2003; Resnik, 2021). The cortical bone is dense and stiff with a Young's modulus (or elastic modulus, denoted as E) in the GPa regime (Peterson et al., 2006; Schwartz-Dabney and Dechow, 2003). The trabecular bone contains sparse bone trabeculae and bone marrow that form a cellular medium with an Young's modulus in the MPa regime (Misch et al., 1999; O'Mahony et al., 2000).

The trabecular bone is "bonded" to the cortical one, and it is also the primarily damageable component of the bone, according e.g. to (Nawathe et al., 2014). Whereas it is quite difficult to pinpoint the exact location of the initial bone damage under load, it appears that part of it is located at the transition (interface) region between the cortical and trabecular bone. The exact amount of trabecular damage will determine the level of mechanical redundancy according to (Fields et al., 2012). From a continuum point of view, the development of trabecular damage is equivalent to an alteration of Young's modulus, and perhaps Poisson's ratio as well, so that damage will apparently reduce both moduli

* Corresponding author.
E-mail address: sagich@technion.ac.il (S. Chen).

https://doi.org/10.1016/j.bonr.2021.101066
Received 2 April 2021; Accepted 6 April 2021

(Kachanov, 1986). Since the work presented here adopts a continuum mechanics perspective without any damage evolution or location, we will just invoke potential damage (either for health and/or mechanical reasons) as the factor dictating variations of the elastic moduli. Moreover, since part of the damage is interfacial, we will make an additional simplification assuming two extreme interfacial states, namely intact (fully bonded) or fully damaged (unbonded).

The alveolar ridge shape and composition is largely maintained by the presence of the teeth. Should any tooth be lost, that portion of the alveolar process that supported the missing tooth will be subject to atrophic reduction (Atwood, 1963; Lamster, 2003). In addition, the use of denture decreases the magnitude of the bite force in denture patients by 4–5 times. This way the stresses and strains experienced by the supporting bone are largely reduced, which triggers structural adaptation to function. The changes are accompanied by changes in material properties both in the maxilla and the mandible. Note that the alveolar bone architecture and shape depend on many parameters, such as the individual's age, health gender, time from extraction, etc. (Lamster, 2003).

Bone strength is determined by a combination of bone quality, quantity, and turnover rate. The biological response to stresses and strains leads to gradual changes in bone shape and/or material properties. For example, loss of bone density decreases bone strength (Natali, 2003).

One finds widely varying values of the bone components' mechanical characteristics to such an extent that it is quite difficult to select a representative value (Dechow et al., 2010; Schwartz-Dabney and Dechow, 2002). One can also find mentions of the bone's Young's modulus (Odin et al., 2010) and density as equivalent to its structural stiffness (Brosh et al., 2014; Collins et al., 2021; Schaffler and Burr, 1988). Such quantification is debatable since the concept of a modulus of elasticity relates to a material property, irrespective of the structural geometry, so that it cannot be considered as the leading mechanical characteristic of the jawbone. Let us note that this distinction was already made by Brunski in his discussion on Misch's work (Brunski, 1999) and in additional references mentioning the jawbone stiffness in relation with dental implants (Brunski and Skalak, 1998; Morgan and James, 1995). Therefore, we distinguish in this paper between the *moduli of elasticity* (Young's and Poisson's) and the *structural normal stiffness* of the jawbone, the latter being a reflection of the combination of shape and architecture together with the material moduli. We will use the results due to Misch (Misch et al., 1999) in this paper as the starting point for the calculations reported in the sequel.

Understanding the biomechanical response of a living bone, whether healthy or not, should start by collecting information regarding the structural and material properties. Shemtov Yona studied the cross-sectional shapes of the alveolar ridges in different areas of the maxilla and mandible and the contribution of the cortical and trabecular bones to the overall shape (both dentate and edentulous). The study, carried out and personally communicated by Shemtov Yona (2021), constructed a typical cross-section of the alveolar ridge in 3 regions of the jaws, starting from the anterior, through the premolar, to the posterior. The outcome of this study presents the bone structure in the spirit of Misch's bone classification (Resnik, 2021) but based on geometrical rather than empirical considerations. This bone type classification becomes particularly relevant for the edentulous jawbone case into which one or more implants are planned to be inserted. However, this new geometrical classification lacks a mechanical interpretation of each bone type, a point that was noted earlier by Brunski in his discussion (Brunski, 1999) of Misch's classification (Misch et al., 1999).

The cortical and trabecular regions are spatially continuous but indeed distinct, generating what could be considered as an artificial interface (uncharacterized so far). In this work, we will assume the transition region to be an interface whose properties dictate the mechanical interaction between the corticular and the trabecular bones.

Consequently, this work evaluates the structural stiffness of the various types of edentulous jawbones according to Shemtov Yona's classification, using a linear elastic, isotropic material model. The influence of the trabecular-cortical interaction on the bone stiffness is parametrically assessed for various values of the elastic moduli in the commonly reported ranges and slightly beyond.

The paper is organized as follows: We first present the numerical model used throughout the paper, including 6 representative edentulous cross-sections of the maxilla and mandible, distinguishing between cortical and trabecular bones. Next, we characterize the stiffness of each bone cross-section, featuring bonded and unbonded bone components for representative values of the bone elastic moduli. The following section characterizes the bone stiffness resulting from a parametric variation of the trabecular bone's Young's modulus in the range of 50 to 200 MPa and a Poisson's ratio in the range of 0.1 and 0.49, keeping the cortical moduli constant.

2. Numerical model

The numerical simulations were carried out using a static finite-element solver (Abaqus/Standard (Simulia, 2020)). The finite-element model was meshed using approximately 50,000 quadrilateral eight-node plane-strain elements, following a preliminary mesh convergence process. The material model assumes linear elasticity with a Young's modulus and Poisson's ratio of 13.5 GPa and 0.2 for the cortical bone (Dechow et al., 2010; Schwartz-Dabney and Dechow, 2002) and 107 MPa and 0.3 for the trabecular (Misch et al., 1999) (Fig. 1). To simplify the amount of data pertaining to the values of the elastic moduli, we will assume that the bone components are isotropic so that only two coefficients are needed to describe their mechanical properties. Calculations were carried out assuming a plane strain configuration. Consequently, the results will be presented after normalization per mm thickness of the bone.

The boundary conditions consist of zero displacements in the vertical direction at the bottom of the bone section, with one fixed node to prevent rigid body motion (see red dot in Fig. 2). A stiff bar is added to the model to replicate in-silico experimental conditions in which the displacement is prescribed. A load-displacement curve is derived according to the bar's displacement (arrows in Fig. 2) and the integrated supporting nodes' reaction (circles in Fig. 2). Finally, the stiffness is obtained from the slope of the load-displacement curve. Note that the force and the bone stiffness are both calculated for 1 mm bone thickness in the out-of-plane direction. The prescribed displacement is infinitesimal throughout all the calculations, hence sufficient to determine the structural stiffness without inducing bone damage.

3. Results

3.1. Bonded and unbonded cases and elastic properties of the components

The load-displacement curves of a bonded and unbonded cases of a cortical-trabecular structure are given in Fig. 3 for three typical cross-sections of the jawbone ridges (maxilla and mandible). For each one of the cross-sections, we compare the three following models: (1) the trabecular bone alone, (2) the cortical bone alone, (3) the cortical-trabecular structure, referred to as "total bone".

The maxilla (Fig. 3a) and mandible (Fig. 3b) ridges' stiffnesses are determined from the load-displacement linear slopes. The bonded case is far stiffer than any other case, irrespective of the jawbone and location. The stiffness of the unbonded bone is somewhat equal to a superposition of cortical plus trabecular stiffnesses. For a specific Young's modulus and Poisson's ratio, this interaction mode represents the softest bone, and thus a lower bound for the structural bone stiffness calculation (damage is not considered). However, considering the bonded model as an upper bound (and more realistic) case, it can be observed that the stiffness is drastically higher and not equal to the sum of the components' stiffnesses.

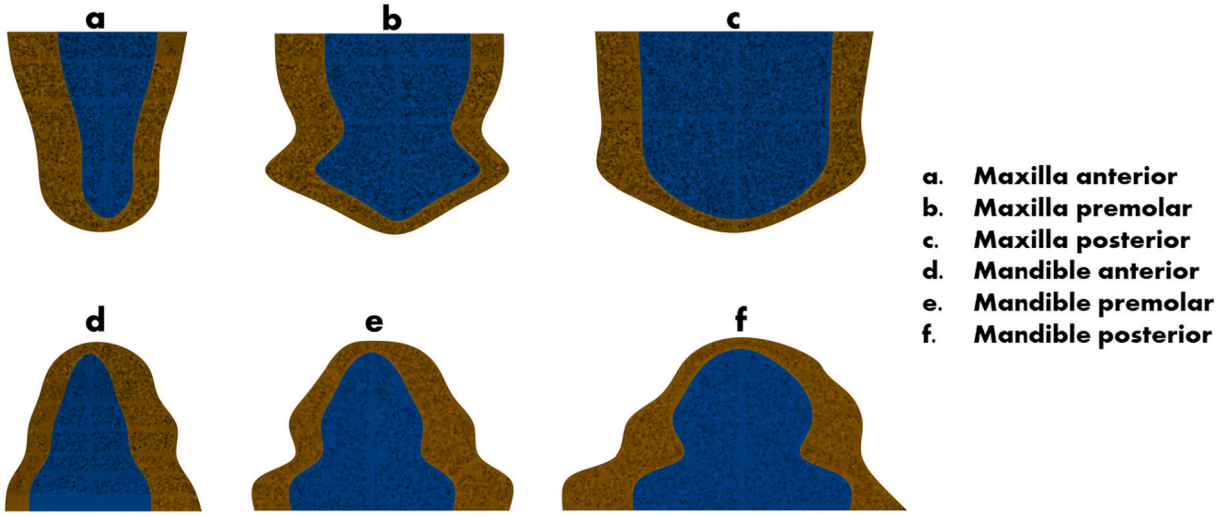

Fig. 1. (a–c) Maxilla and (d–f) mandible ridges, classified by their dimensions, according to Shemtov Yona (2021).

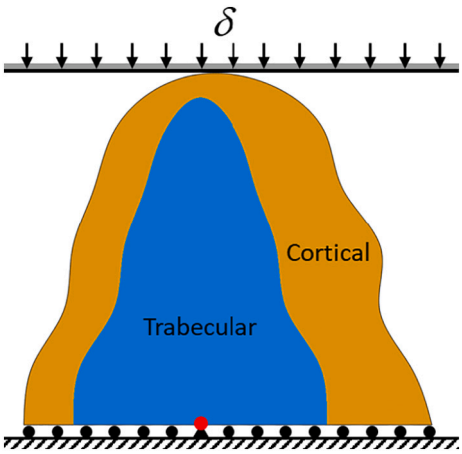

Fig. 2. Boundary condition illustrated in a representative model of the mandible anterior cross-section. A stiff bar is lowered by δ displacement. The bone is compressed between the bar and the supports that allow motion in the horizontal direction, with one fixed node (marked red) to prevent rigid body motion. The cortical and trabecular bone components can be fully bonded or unbonded.

Fig. 4 summarizes the above results for the stiffness of each bone case with a 1 mm out of plane thickness. A clear decrease in stiffness from anterior to posterior areas was observed both for the maxilla and the mandible. The stiffness decreases nonlinearly in the maxilla from anterior to posterior, whereas for the mandible, the decrease is nearly linear.

In order to get a refined understanding of the influence of the interfacial constraint between the bone components with different material properties, the anterior mandible model is shown in its initial ("undeformed" in Fig. 5a) and deformed (Fig. 5b, c) configuration for both interaction modes – bonded and unbonded – both for the same displacement of $\delta = 1\mu m$. The illustration of the deformed configurations in Fig. 5b, c are magnified 10 times to show the gap between the separated regions, leaving a small region of active interaction at the top of the interface, see the close-up in Fig. 5c. This figure shows that unlike the bonded case, the gap opening in the unbonded case allows for load transfer through a significantly reduced contact at the apical area.

3.2. *Effect of trabecular elastic moduli*

The following section characterizes the bone stiffness resulting from a parametric variation of the trabecular bone's Young's modulus in the range of 50 to 200 MPa, and Poisson's ratio in the range of 0.1 and 0.49, keeping the cortical moduli constant. The influence of the trabecular bone elastic properties on the overall bone stiffness is analyzed next. The bone stiffness is calculated for different combinations of Young's modulus (Fig. 6a, b) and Poisson's ratio (Fig. 6c, d). As before, we distinguish between the bonded and unbonded interfacial constraints, as shown in Fig. 6, keeping in mind that the unbonded stiffness is almost equal to the cortical stiffness itself.

Similar to the trends shown in Fig. 4, the bone stiffness increases linearly from the anterior to the posterior with both Poisson's ratio and Young's modulus in the mandible, whereas this is not the case for the maxilla where the anterior stiffness is markedly superior to all other stiffnesses. Finally, one notes that the posterior and premolar unbonded cases of the maxilla appear to have a stiffness that is independent of the value of the elastic moduli.

3.2.1. *Effect of Young's modulus*

Considering the bonded case, it is found that the stiffness increases markedly with the Young's modulus. Similar trends (almost linear) are observed for both the mandible and the maxilla, and as before, the unbonded case is not much influenced by changing the Young's modulus.

3.2.2. *Effect of Poisson's ratio*

Up to a value of ca. 0.3, Poisson's ratio has no significant influence for both bonded and unbonded cases, however, the bone stiffness increases markedly past this value, especially in the mandible-bonded cases.

4. Discussion

The jawbone stiffness is evaluated for representative cross-sections of edentulous maxilla and mandible alveolar processes adopting the geometric classification of Shemtov Yona (2021). From a mechanical point of view, the bone combines two different regions that totally differ in elastic properties. We model the two bone components as separate regions with an interaction to reflect the smooth transition from the highly porous trabecular to the much denser cortical. We did not explicitly consider bone failure so that the two extreme cases shown here examine the combined influence of the elastic moduli and bone geometry on the bone stiffness. It worth noting that a high-resolution investigation of the trabecular bone should be employed when looking for local bone damaging or when accounting for large deformations, keeping in mind

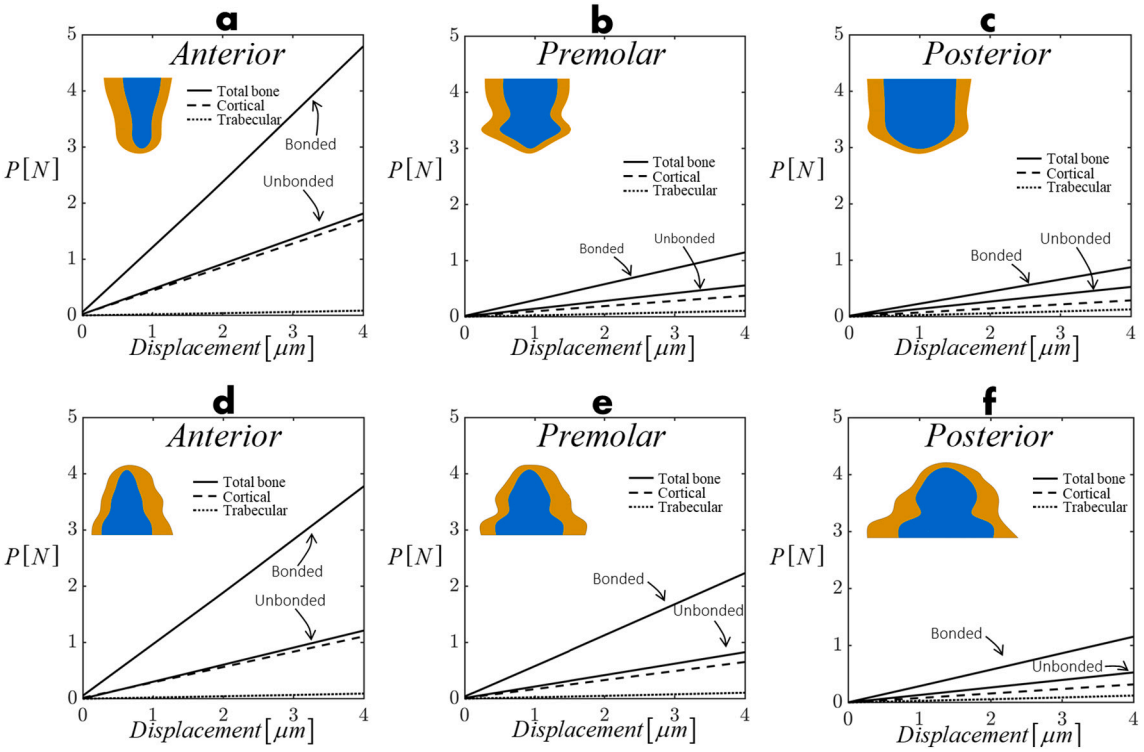

Fig. 3. Load-displacement curves of (a) maxilla anterior, (b) maxilla premolar, (c) maxilla posterior, (d) mandible anterior, (e) mandible premolar, (f) mandible posterior. Bonded and unbonded cases. The scale is deliberately identical for all the cases. Forces are reported for a 1 mm thick bone slice.

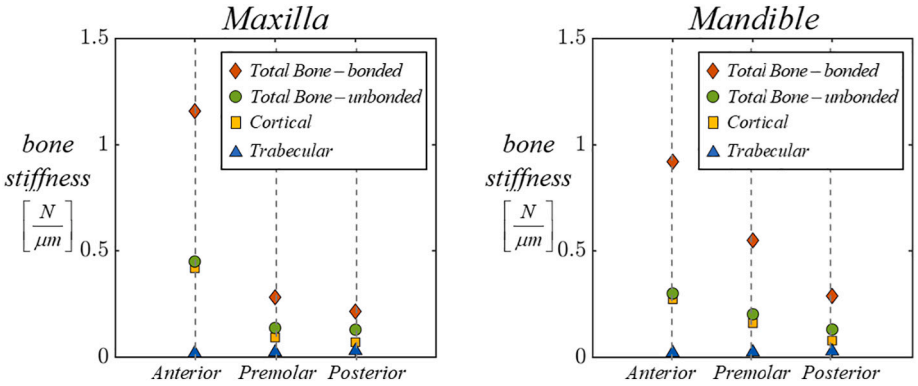

Fig. 4. The stiffness normalized by the thickness of the cross-sections of the (a) maxilla and the (b) mandible jawbones. "Bonded" and "unbonded" refer to the two limit cases of cortical/trabecular interaction property.

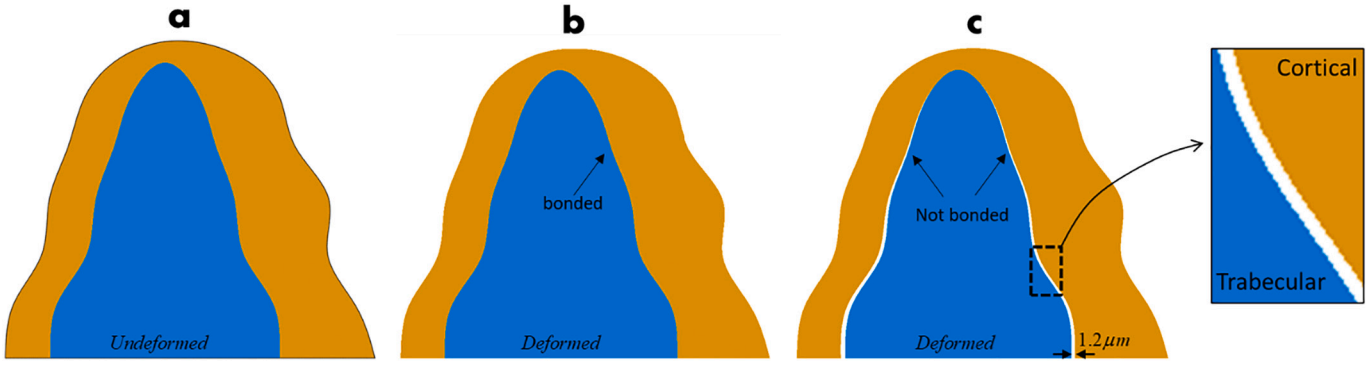

Fig. 5. (a) Undeformed and (b, c) deformed configurations of the anterior mandible model. In (c), the cortical and trabecular regions are unbonded and thus separating while loaded. The deformed cases are for a similar displacement of 1 μm.

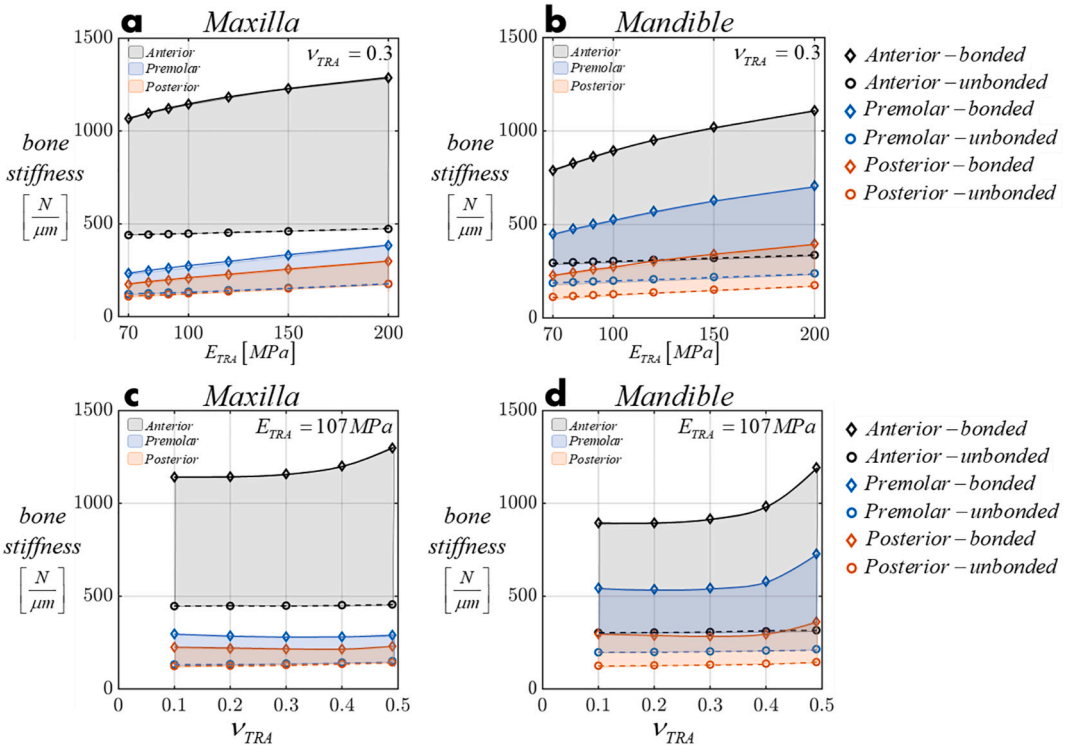

Fig. 6. In (a, b), the bone stiffness is given for different Young's modulus values ranging from 70 to 200 MPa with a similar Poisson's ratio of 0.3. In (c, d), the bone stiffness is given for different Poisson's ratio ranging from 0.1 to 0.49 with a similar Young's modulus of 107 MPa.

that fracture initiation strongly depends on the geometry and thus on the specific model resolution (Nawathe et al., 2014). It is clear that the bonded case is much closer to the clinical reality than the unbonded case, the latter being reported here such as to set up bounds for the bone stiffness.

It should be kept in mind that we model reduced cross sections of the ridge, according to the geometrical information found in the literature that does not extend beyond 6 mm in depth. The reported results are therefore to be considered for their trends rather than absolute values. Yet, when considering the results of measurements carried out by Brosh et al. (Brosh et al., 2014) on the stiffness of porcine mandible cortical bone (1.5 mm thick), the measured stiffness is of the order of 0.35–0.91 N/μm which is definitely in agreement with our calculated values, after normalization by the thickness (Fig. 4). For the trabecular bone, various relationships have been established between the elastic modulus and the bone density (without distinction here between ash or mineral), as in (Carter and Hayes, 1977). This relationship is important for the clinical community who considers bone density as a prime property and general indication of the bone strength.

We examined various pairs of elastic moduli (Young's modulus, E, and Poisson's ratio, ν) for the trabecular medium and two extreme cases for the interaction property between the cortical and trabecular regions – bonded, and frictionless unbonded. In both limit cases, the stiffness rises with any trabecular Young's modulus in the tested range. On the other hand, the Poisson's ratio is influential when exceeding the value of $\nu = 0.3$ towards the incompressible value of $\nu = 0.5$. For comparable cross-sections, the maxilla exhibits greater differences in stiffness when compared with the mandible for both E and ν. Generally, the structural stiffness of the alveolar process is shown to decrease with location from anterior to posterior, with a strong dependence on the cross-section shape rather than on differences in the elastic moduli. When unbonded, the cortical shell bears most of the loading, and the stiffness is in the range of the sole cortical component. In the bonded case, the trabecular medium exerts lateral restraint through its Poisson's ratio, that significantly stiffens the bone assembly above the mere summation of its components' stiffnesses, thus revealing a significant stiffening synergy.

One may suggest that the concept of structural redundancy proposed by (Fields et al., 2012), which states that if some failure occurs in the trabecular bone, an alternate loading path may be found that preserves structural functionality, may now be explicitly related to interfacial trabecular failure for being of prime importance for the structural stiffness. Yet, this necessitates future studies on the structural properties of the bone, and more specifically, the failure mechanism of the trabecular medium.

As a final remark, beyond its mechanical interpretation, the present work also bears clinical implications as a starting point. The various bone sections are now characterized mechanically in addition to their earlier geometrical classification, so that the outcome of adding a dental implant can be modelled next, and the resulting structural stiffness be calculated in relation with the implant stability. The latter is often clinically asserted through forced vibrational techniques, e.g. Resonant Frequency Analysis (Rittel et al., 2019; Sennerby and Meredith, 2008), or using ultrasound -QUS- (Dorogoy et al., 2020; Vayron et al., 2018). In those techniques, the outcome is dictated by the implant structure, its degree of bonding to the bearing bone, and also to the shape and structure of the supporting bone slice altogether. In that context, the concept of initial bone-implant micromotions (Winter et al., 2013) is also directly influenced, not only by the quality of the bone-implant bond but also by the stiffness of the supporting tissue.

5. Conclusions

The structural stiffness of the alveolar process varies with location in the jawbone.

The structural stiffness is a function of the bone geometry, the elastic properties of its components and their interaction.

The interaction between the cortical and the trabecular components causes a synergistic increase of the structural stiffness that goes way beyond the mere sum of the individual components' stiffnesses.

As such, the role of the very soft trabecular bone in the mechanical

assembly is not negligible.

The calculated bone stiffness adds a mechanical insight to the new geometrical classification of the jawbone cross-sections of Shemtov Yona (2021).

The present results can also be applied to the characterization of dental implants' stability as a function of their placement.

Declaration of competing interest

The authors declare that they have no known competing financial interests or personal relationships that could have appeared to influence the work reported in this paper.

References

Atwood, D.A., 1963. Postextraction changes in the adult mandible as illustrated by microradiographs of midsagittal sections and serial cephalometric roentgenograms. J. Prosthet. Dent. 13, 810–824.

Brosh, T., Rozitsky, D., Geron, S., Pilo, R., 2014. Tensile mechanical properties of swine cortical mandibular bone. PLoS One 9, 1–11. https://doi.org/10.1371/journal.pone.0113229.

Brunski, J.B., 1999. Mechanical properties of trabecular bone in the human mandible: implications for dental implant treatment planning and surgical placement. J. Oral Maxillofac. Surg. 57, 706–708.

Brunski, J.B., Skalak, R., 1998. Biomechanical considerations for craniofacial implants. Osseointegr. Craniofacial Reconstr. 15–35.

Carter, D.R., Hayes, W.C., 1977. The compressive behavior of bone as a two-phase porous structure. J Bone Jt. Surg. 7, 954–962. https://doi.org/10.1007/978-1-4471-5451-8_116.

Collins, C.J., Yang, B., Crenshaw, T.D., Ploeg, H.L., 2021. Evaluation of experimental, analytical, and computational methods to determine long-bone bending stiffness. J. Mech. Behav. Biomed. Mater. 115, 104253. https://doi.org/10.1016/j.jmbbm.2020.104253.

Dechow, P.C., Wang, Q., Peterson, J., 2010. Edentulation alters material properties of cortical bone in the human craniofacial skeleton: functional implications for craniofacial structure in primate evolution. Anat. Rec. (Hoboken). 293, 618–629. https://doi.org/10.1002/ar.21124.

Dorogoy, A., Haïat, G., Shemtov-Yona, K., Rittel, D., 2020. Modeling ultrasonic wave propagation in a dental implant - bone system. J. Mech. Behav. Biomed. Mater. 103, 103547. https://doi.org/10.1016/J.JMBBM.2019.103547.

Fields, A.J., Nawathe, S., Eswaran, S.K., Jekir, M.G., Adams, M.F., Papadopoulos, P., Keaveny, T.M., 2012. Vertebral fragility and structural redundancy. J. Bone Miner. Res. 27, 2152–2158. https://doi.org/10.1002/jbmr.1664.

Kachanov, L.M., 1986. Introduction to continuum damage mechanics. Continuum Damage Mechanics of Materials and Structures. https://doi.org/10.1016/b978-008043918-1/50038-1.

Lamster, I.B., 2003. Clinical periodontology and implant dentistry, Fourth Edition, sixth edit. ed. J. Dent. Res. https://doi.org/10.1177/154405910308201117. Wiley-Blackwell.

Misch, C.E., Qu, Z., Bidez, M.W., 1999. Mechanical properties of trabecular bone in the human mandible: implications for dental implant treatment planning and surgical placement. J. Oral Maxillofac. Surg. 57, 700–706. https://doi.org/10.1016/S0278-2391(99)90437-8.

Morgan, M.J., James, D.F., 1995. Force and moment distributions among osseointegrated dental implants. J. Biomech. 28, 1103–1109. https://doi.org/10.1016/0021-9290(94)00139-U.

Natali, A.N., 2003. Dental Biomechanics. Taylor & Francis.

Nawathe, S., Akhlaghpour, H., Bouxsein, M.L., Keaveny, T.M., 2014. Microstructural failure mechanisms in the human proximal femur for sideways fall loading. J. Bone Miner. Res. 29, 507–515. https://doi.org/10.1002/jbmr.2033.

Odin, G., Savoldelli, C., Bouchard, P.O., Tillier, Y., 2010. Determination of Young's modulus of mandibular bone using inverse analysis. Med. Eng. Phys. 32, 630–637. https://doi.org/10.1016/j.medengphy.2010.03.009.

O'Mahony, A.M., Williams, J.L., Katz, J.O., Spencer, P., 2000. Anisotropic elastic properties of cancellous bone from a human edentulous mandible. Clin. Oral Implants Res. 11, 415–421. https://doi.org/10.1034/j.1600-0501.2000.011005415.x.

Peterson, J., Wang, Q., Dechow, P.C., 2006. Material properties of the dentate maxilla. Anat. Rec. Part a. Discov. Mol. Cell. Evol. Biol. 288, 962–972. https://doi.org/10.1002/ar.a.20358.

Resnik, R., 2021. Contemproray Implant Dentistry. Hilos Tensados.

Rittel, D., Dorogoy, A., Haïat, G., Shemtov-Yona, K., 2019. Resonant frequency analysis of dental implants. Med. Eng. Phys. 65–74.

Schaffler, M.B., Burr, D.B., 1988. Stiffness of compact bone: effects of porosity and density. J. Biomech. 21, 13–16. https://doi.org/10.1016/0021-9290(88)90186-8.

Schwartz-Dabney, C.L., Dechow, P.C., 2002. Edentulation alters material properties of cortical bone in the human mandible. J. Dent. Res. 81, 613–617. https://doi.org/10.1177/154405910208100907.

Schwartz-Dabney, C.L., Dechow, P.C., 2003. Variations in cortical material properties throughout the human dentate mandible. Am. J. Phys. Anthropol. 120, 252–277. https://doi.org/10.1002/ajpa.10121.

Sennerby, L., Meredith, N., 2008. Implant stability measurements using resonance frequency analysis: biological and biomechanical aspects and clinical implications. Periodontol. 2000 (47), 51–66. https://doi.org/10.1111/j.1600-0757.2008.00267.x.

Shemtov Yona, K., 2021. Personal Communication.

Simulia, D.S., 2020. Abaqus 2020. Abaqus Anal. User's Guid.

Stanley, N.J., Major, A.M., 2010. Wheeler's Dental Anatomy, Physiology and Occlusion. Acta Universitatis Agriculturae et Silviculturae Mendelianae Brunensis.

Vayron, R., Nguyen, V.-H., Lecuelle, B., Albini Lomami, H., Meningaud, J.-P., Bosc, R., Haiat, G., 2018. Comparison of resonance frequency analysis and of quantitative ultrasound to assess dental implant osseointegration. Sensors 18, 1397. https://doi.org/10.3390/s18051397.

Winter, W., Klein, D., Karl, M., 2013. Micromotion of dental implants: basic mechanical considerations. J. Med. Eng. 2013, 1–9. https://doi.org/10.1155/2013/265412.